

Citation for published version:
Baardink, G, Cassella, G, Neville, L, Milewski, PA & Souslov, A 2021, 'Complete absorption of topologically protected waves', *Physical Review E*, vol. 104, no. 1, 014603. https://doi.org/10.1103/PhysRevE.104.014603

DOI:

10.1103/PhysRevE.104.014603

Publication date: 2021

Document Version Peer reviewed version

Link to publication

University of Bath

Alternative formats

If you require this document in an alternative format, please contact: openaccess@bath.ac.uk

Copyright and moral rights for the publications made accessible in the public portal are retained by the authors and/or other copyright owners and it is a condition of accessing publications that users recognise and abide by the legal requirements associated with these rights.

Take down policy
If you believe that this document breaches copyright please contact us providing details, and we will remove access to the work immediately and investigate your claim.

Download date: 12 Mar 2023

Complete absorption of topologically protected waves

Guido Baardink, ¹ Gino Cassella, ¹ Luke Neville, ¹ Paul A. Milewski, ² and Anton Souslov^{1, *}

¹ Department of Physics, University of Bath, Claverton Down, Bath, BA2 7AY, UK

² Department of Mathematical Sciences, University of Bath, Claverton Down, Bath, BA2 7AY, UK

(Dated: October 16, 2020)

Chiral edge states can transmit energy along imperfect interfaces in a topologically robust and unidirectional manner when protected by bulk-boundary correspondence. However, in continuum systems, the number of states at an interface can depend on boundary conditions. Here we design interfaces that host a net flux of the number of modes into a region, trapping incoming energy. As a realization, we present a model system of two topological fluids composed of counter-spinning particles, which are separated by a boundary that transitions from a fluid-fluid interface into a no-slip wall. In these fluids, chiral edge states disappear, which implies non-Hermiticity and leads to a novel interplay between topology and energy dissipation. Solving the fluid equations of motion, we find explicit expressions for the disappearing modes. We then conclude that energy dissipation is sped up by mode trapping. Instead of making efficient waveguides, our work shows how topology can be exploited for applications towards acoustic absorption, shielding, and soundproofing.

When does broken time-reversal symmetry imply non-Hermiticity? The converse is always true, because gains and losses in non-Hermitian Hamiltonians break thermodynamic reversibility and time-reversal symmetry [1– 18]. By contrast, transverse velocity-dependent forces, although odd under time reversal, do converse energy and preserve Hermiticity. Examples of these Hermitian effects include Lorentz forces due to an applied magnetic field [19], Coriolis forces due to an external rotation [20– 22], and so-called odd (Hall) viscosity [23–29] arising in exotic quantum and classical fluids. In gapped Hermitian systems, broken time-reversal symmetry is associated with a wealth of topological phenomena such as unidirectional interface states protected against scattering. Such chiral interface modes are guaranteed to accompany any jump in a topological invariant called the Chern number due to bulk-interface correspondence [19, 30]. These robust edge states have been proposed and realized across a variety of electronic [19, 31–33], photonic [34–37], and mechanical [20, 21, 29, 30, 38–48] systems.

In continuum fluids, bulk-boundary correspondence requires additional ingredients [49–52] and can be even be violated [53]. We consider the continuum topological system in two dimensions illustrated in Fig. 1(a). The container includes an interface between two counterrotating chiral active fluids composed of self-rotating particles (equivalently, active rotors), each spinning with an intrinsic rotation rate $\pm\Omega_A$ [54–64]. In addition, either through external forces or internal active stresses [54–64], the fluid flow is characterized by vorticity $\pm \Omega_B$. This example relies on the commonly observed segregation of oppositely rotating chiral active particles [65–69]. These fluids exhibit bulk acoustic band gaps, which in the presence of active rotation can be characterized by topological Chern number $C=\pm 2$ [29]. The dashed middle line denotes a fluid-fluid (i.e., stress continuity) boundary, at which bulk-boundary correspondence holds [21, 70], resulting in 4 (four) interface modes. Along the right-most

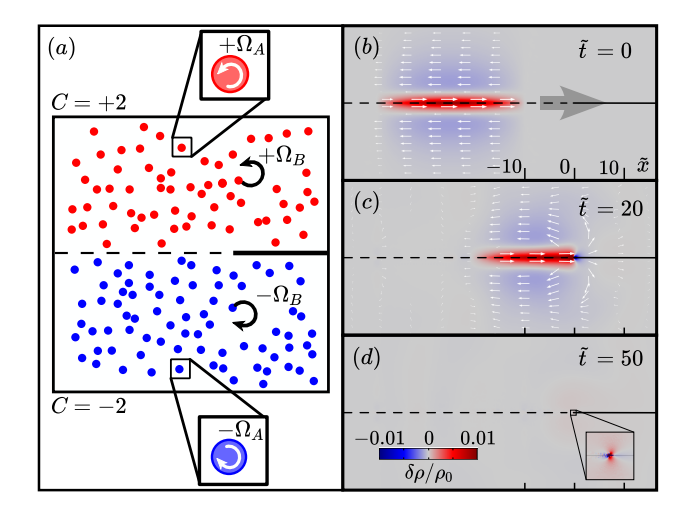


FIG. 1. Completely absorbed interface mode in a chiral active fluid. (a) Schematic a two-dimensional system of two chiral active fluids composed of counter-rotating particles. Each particle spins with rotational speed $\pm\Omega_A$ and is subject to a Coriolis force density $\pm \Omega_B v^*$, where v^* is the velocity v rotated by 90°. The bulk is gapped with topological invariant $C = \operatorname{sgn}(\Omega_A) + \operatorname{sgn}(\Omega_B)$. The interface between the two fluids supports right-moving edge modes, one of which is shown in (b)-(d). (b) The right-moving pulse along the fluid-fluid interface (dotted line). (c) The pulse hits the no-slip wall (solid line). (d) The pulse is completely absorbed. Density differences $\delta \rho$ around an equilibrium density ρ_0 are shown in color, and the velocity field is portrayed by white arrows. Time $\tilde{t} = t/T$ and space $\tilde{x} = x/L$ are nondimensionalized by $L \equiv |\nu^{o}|/c$ and $T \equiv |\nu^{o}|/c^{2}$, using the odd viscosity parameter $\nu^{\circ} \sim \Omega_A$, see text. The incoming wave has parameters $\Omega_B T = 1/5$ and $\omega T = qL = \pi/30$.

segment, we imagine a thin rigid slab is inserted and the boundary conditions change to a no-slip interface (denoted by a solid line), at which the velocity vanishes.

In this work, we use analytical solutions to show that the no-slip interface does not respect bulk-boundary correspondence and supports instead only 2 (two) interface modes. We find that in such systems, the simultaneous breaking of time-reversal and bulk-boundary correspondence guarantees non-Hermiticity. Figure 1(b-d) shows snapshots for a mode propagating along the fluid-fluid interface. Because this mode is orthogonal to any that exist on the no-slip interface, the mode is completely absorbed, vanishing once it reaches the change in boundary, Fig. 1(d). In a Hermitian system, such energy dissipation is prohibited, and no consistent solution exists. To resolve this apparent paradox, we are forced to include non-Hermitian dissipative viscosity in this topological theory. First, we present a general argument for when the non-Hermitian dissipative terms must be included in a theory of chiral edge states, by counting fluxes of mode numbers into a region.

Topological flux trapping— Provided that the equations of motion are linear and have wave-like solutions, mode flux trapping [e.g., Fig. 1(b-d)] occurs when two exotic conditions are satisfied: the system must (i) break time-reversal symmetry and (ii) violate bulk-interface correspondence. (i) Time-reversal symmetry (in this case equivalent to reciprocity) implies that for every rightmoving wave at wavevector \boldsymbol{q} and frequency $\omega(\boldsymbol{q})$ there exists a left-moving wave with equal frequency $\omega(-q)$. Then, through every boundary there is an equal number of modes flowing in each direction, Fig. 2(a-b). Therefore, the net number of modes going into any region is zero. (ii) In non-reciprocal systems which satisfy bulkinterface correspondence, the net flux of modes into a region is still zero. This is because topological protection guarantees that for each incoming wave, there exists an outgoing wave along the same boundary at the opposite end, Fig. 2(c).

Chiral active fluids satisfy both of these conditions and can have the interface mode structure depicted in Fig. 2(d). As a consequence, more modes enter a region than can leave. The net flux of modes Φ into a region can be evaluated using the expression

$$\Phi = \sum \operatorname{sgn}(\boldsymbol{q} \cdot \hat{\boldsymbol{n}}), \tag{1}$$

which sums the signed number $\operatorname{sgn}(\boldsymbol{q}\cdot\hat{\boldsymbol{n}})$ of modes flowing into a region over all of the boundary elements. In analogy with typical expressions for a flux, the quantity $\operatorname{sgn}(\boldsymbol{q}\cdot\hat{\boldsymbol{n}})$ acts as a vector field dotted into a surface normal. However, this quantity can only be an integer because it corresponds to a mode count for flow either into (contributing flux 1) or out of (contributing flux -1) the region. The mode flux Φ for the geometry in Fig. 2(d) is positive and can be evaluated as the sum of fluxes at the two points L/R where the interface crosses the boundary of the region

$$\Phi = \Phi_L + \Phi_R = (N_L^{in} + N_R^{in}) - (N_L^{out} + N_R^{out}), \quad (2)$$

where $N_{L/R}^{in/out}$ is the number of modes flowing into/out

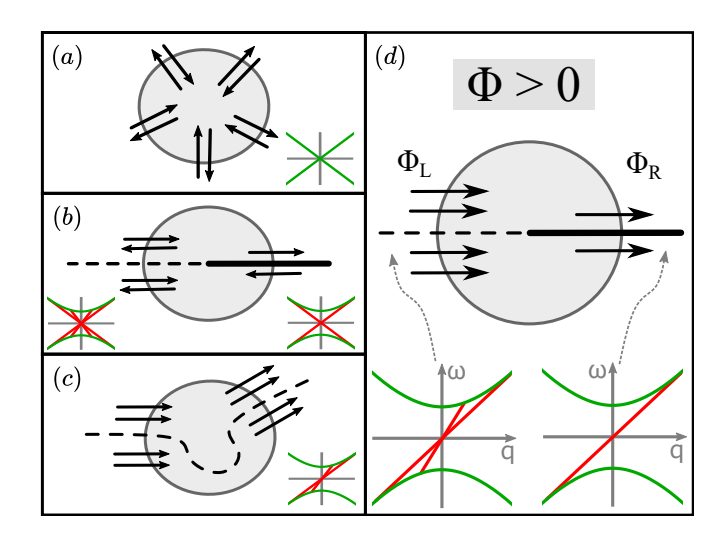


FIG. 2. Mode absorption and non-Hermiticity. In a region of space (grey circle), we count the number of in- and out-flowing modes (black arrows) and apply the pigeonhole principle. Insets in (a-d) show different bulk (green) and interface (red) dispersion relations. (a) Ungapped time-reversal-symmetric system. Every in-flowing mode is paired with a mode flowing out by time-reversal symmetry (TRS). The net mode flux Φ is zero. (b-d) Gapped systems, for which $\Phi = \Phi_L + \Phi_R$, where $\Phi_{L/R}$ counts modes at the two points where the interface (dotted/solid lines) crosses the region's boundary. (b) Gapped system with TRS. $\Phi_L = \Phi_R = 0$, even if BCs change the number of interface modes. (c) System for which TRS is broken, but bulk-interface correspondence holds. Topological protection guarantees one out-flowing mode for each inflowing mode, even along complex interfaces, $\Phi_L + \Phi_R = 0$. (d) When both TRS and bulk-interface correspondence are broken, the in-flowing modes can outnumber the out-flowing modes, so that $\Phi > 0$ and non-Hermiticity is guaranteed.

of a region through the point L/R.

We now show that for traveling waves, a positive mode flux (i.e., $\Phi > 0$) necessitates non-Hermitian physics. We do so by defining an $N^{in} \times N^{out}$ rectangular extension \tilde{S} of the scattering matrix that maps incoming waves into outgoing waves, assuming no bound states. For $\Phi > 0$, a theorem of linear algebra states that the rectangular matrix \hat{S} must map at least Φ independent modes to zero [71]. This observation precludes a description of the dynamics in terms of a purely Hermitian Hamiltonian \mathcal{H} , which would instead imply a (typical) unitary scattering matrix $S \equiv e^{i\mathcal{H}}$ that cannot map any nonzero modes to zero. This extension of scattering matrices outside the unitary group is typical of non-Hermitian dynamics [72– 76] and systems defined by information loss, including black holes [77]. In summary, the topological physics associated with a positive mode flux Φ needs to be regularized by dissipative non-Hermiticity.

As a toy model for regularization by dissipation, consider a reduced equation for a single chiral edge mode ψ in one spatial dimension x, $(\partial_t - \partial_x)\psi = \nu \partial_x^2 \psi$ with a nonzero initial condition for $\psi(x < 0)$ and the bound-

ary condition $\psi(0)=0$, which ensures that ψ "vanishes" for positive x. Around the origin, $\Phi>0$, and no bound modes are allowed. For $\nu=0$, the solution $\psi(x-t)$ cannot be valid for all time. By contrast, for $\nu>0$, the boundary condition remains compatible with the chiral edge mode.

Hydrodynamic theory with vanishing modes— One minimal two-band model for violating bulk-boundary correspondence is a compactified Dirac cone [53]. We instead demonstrate the flux-trapping mechanism using the hydrodynamic description of chiral active fluids [29]:

$$\partial_t \mathbf{v} + \nabla \rho = -s(m + \nabla^2) \mathbf{v}^* + \nu \nabla^2 \mathbf{v},$$

$$\partial_t \rho + \nabla \cdot \mathbf{v} = D \nabla^2 \rho,$$
 (3)

where $\mathbf{x} \equiv (x, y)$, $\mathbf{v} \equiv (u, v)$, and $\mathbf{v}^* \equiv (-v, u)$, with an interface at y = 0 with $s = \operatorname{sgn}(y)$. The linearized Eqs. (3) describe the time-evolution of fluid density $\rho_0 + \rho(\mathbf{x}, t)$ and flow velocity $\mathbf{v}(\mathbf{x}, t)$. The left-hand side of Eqs. (3) describes sound waves in a simple fluid.

The term $s(m + \nabla^2)v^*$ in Eqs. (3) describes the hydrodynamic effects due to active rotations of individual particles and active flows. Within this chiral active fluid, each particle spins with intrinsic angular momentum L = $I\Omega_A$ (where Ω_A is the angular velocity and I is the moment of inertia). In addition, each particle feels a Coriolis (or, equivalently, Lorentz) body force $\mathbf{F} = \rho_0 \Omega_B \mathbf{v}^*$, for example due to rotational flow with constant vorticity Ω_B induced by active stresses [28, 29, 64]. In the Supplemental Material (SM), we detail how Eqs. (3) describe sound waves in a chiral active fluid, rescaled using the speed of sound c for the velocities, equilibrium fluid density ρ_0 for the density field, as well as quantities $I\Omega_A/(2c\rho_0)$ and $I\Omega_A/(2c^2\rho_0)$ for length and time, respectively. Active forces can determine the sign of both intrinsic rotation rate Ω_A and cyclotron frequency Ω_B , so we consider cases for which these quantities have the same sign $s = \pm 1$, i.e., $s \equiv \operatorname{sgn}(\Omega_A) = \operatorname{sgn}(\Omega_B) \neq 0$. Due to intrisic particle rotations, the stress tensor contains off-diagonal odd (or Hall) viscosity $\nu^o = I\Omega_A/(2\rho_0)$ (and we measure dissipative viscosity ν in units of ν^{o}). Odd viscosity is a transverse non-dissipative response that results from the simultaneous breaking of parity and time-reversal symmetry [24, 25, 78] in chiral active fluids [26, 28, 79], appearing also in quantum fluids and plasmas [23, 27, 80– 84] as well as rotated gases [85]. The non-dimensionalized form of the fluid stress is $\sigma_{ij} = -\rho \delta_{ij} - s \partial_i v_j^*$ [26, 79]. In these units, the effects of activity are captured by the non-dimensionalized parameter m, given by m = $|I\Omega_A\Omega_B|/(2\rho_0c^2)$. Without odd viscosity, Eqs. (3) also describe waves on the surface of the ocean near the equator or next the shore [22, 86–89].

In Eqs. (3), we have included two non-Hermitian terms: a dissipative viscosity ν and a diffusion coefficient D. We proceed to show by contradiction that such dissipative terms must be included for the equations to be

well posed. We first assume that $\nu=D=0$ and provide details in the SM for solutions to the equations along the interfaces shown in Fig. 1. Bulk solutions to Eqs. (3) can be decomposed into three bands $\omega(q)$. To perform the topological analysis we note that (i) the equations are gapped at low frequencies, and no bulk waves exist in the gap [21, 29, 53, 70]. (ii) The presence of odd viscosity compactifies the fluid's acoustic spectrum [49–52], which allows for the definition of a topological invariant called the Chern number C. For Eqs. (3), $C_s = \mathrm{sgn}(\Omega_A) + \mathrm{sgn}(\Omega_B) = 2s$ (see SM), only defined when both Ω_A and Ω_B are nonzero. The standard bulk-boundary correspondence would suggest the existence of $C_+ - C_- = 4$ modes at any interface between systems with opposite values of s.

By characterizing waves at interfaces, we show that this bulk-interface correspondence does not hold for no-slip boundary conditions. At an interface, we find solutions of the form $(\rho, u, v)^T = \Psi_{\uparrow} e^{i(\omega t - qx)} e^{-\kappa_{\uparrow}|y|}$, assuming $\omega < m$ (i.e., the frequency is in the gap set by Ω_B) and m < 1/4. For each halfspace, which we label \uparrow , we find two solutions, which we denote by ψ_{\uparrow}^{\pm} . The general solution to Eq. (3) has the form $\psi = A_{\uparrow}^+ \psi_{\uparrow}^+ + A_{\uparrow}^- \psi_{\uparrow}^- + A_{\downarrow}^+ \psi_{\downarrow}^+ + A_{\downarrow}^- \psi_{\downarrow}^-$, where the amplitudes A_{\downarrow}^{\pm} must be chosen to satisfy the interface boundary conditions (BCs). The BCs will only satisfy energy conservation if $\hat{\boldsymbol{n}} \cdot \boldsymbol{\sigma} \cdot \boldsymbol{v}|_{y \downarrow 0} = \hat{\boldsymbol{n}} \cdot \boldsymbol{\sigma} \cdot \boldsymbol{v}|_{y \uparrow 0}$, as we review in the SM. Two such interface conditions are (see Figs. 1,3):

Fluid-Fluid (FF):
$$0 = [u] = [v] = [\sigma_{21}] = [\sigma_{22}]$$

No-Slip (NS): $0 = [u] = [v] = \bar{u} = \bar{v}$

$$(4)$$

where we denote by $[u] = u(0^+) - u(0^-)$ the jump across (and by $\bar{u} = (u(0^+) + u(0^-))/2$ the average of) the velocities and stresses at y = 0. As usual, at a fluid-fluid interface the stress is continuous and at a no-slip interface, the velocity vanishes. For each boundary condition, the coefficients A_{\downarrow}^{\pm} of the general solution are related by a single matrix equation $MA_{\downarrow}^{\pm} = \mathbf{0}$. We find the dispersion curves for the interface modes using det M = 0.

Both interface conditions have well posed solutions, even without dissipation. For the fluid-fluid interface, we find four solutions at each frequency ω in the gap, in agreement with bulk-interface correspondence (Fig. 3). These solutions fall into one of two categories: (i) two so-called Kelvin modes with linear dispersion $\omega=q$ and horizontal (v=0) flow; and (ii) two Yanai modes with $|\omega|\neq q$ and purely rotational ($u\propto iv$) flow. For Kelvin modes, the explicit solutions (derived in SM) are $(\rho,u,v)_{K_{1,2}}=(1,1,0)K_{1,2}(y)e^{i\omega(x-t)}$, where the y-profiles $K_{1,2}(y)$ can be orthogonalized as

$$K_{1}(y) = \sinh\left(\frac{1}{2}\Gamma|y|\right) e^{-\frac{1}{2}|y|},$$

$$K_{2}(y) = \left[\cosh\left(\frac{1}{2}\Gamma|y|\right) - \frac{1}{\Gamma}\sinh\left(\frac{1}{2}\Gamma|y|\right)\right] e^{-\frac{1}{2}|y|},$$
(5)

with $\Gamma(\omega) = \sqrt{1-4m+4\omega^2}$. By contrast, for the noslip interface, no Yanai modes exist in the gap and there are again two orthogonal Kelvin modes $\{K_1, K_1^a\}$, where $K_1^a(y) = \operatorname{sgn}(y)K_1(y)$ is the antisymmetrization of K_1 about the interface. This total count of 2 interface modes differs from the jump in Chern number across the interface, which is 4. This discrepancy suggests an apparent violation of the usual bulk-interface correspondence.

The extended scattering matrix \tilde{S} for the fluid-fluid to no-slip transition sends K_1 to itself and annihilates K_2 . We characterize this scattering via symmetry arguments and finite-element simulations of Eqs. (3). For the symmetry argument, consider the parity under reflection $y \to -y$ for components of each mode:

	Fluid-fluid		No-slip	
	K_1, K_2	Y_1, Y_2	K_1	K_1^a
ρ, u	even	odd	even	odd
v	zero	even	zero	zero

Because inner products between waves with opposite parity vanish, we decompose \tilde{S} into odd and even parts, i.e., $\tilde{S}:\langle Y_1,Y_2\rangle \to \langle K_1^a\rangle$ and $\tilde{S}:\langle K_1,K_2\rangle \to \langle K_1\rangle$. The even-parity sector indeed maps mode K_1 onto itself and annihilates the orthogonal mode K_2 , which we observe in simulations, Fig. 3. This completes our contradiction: when $\nu=D=0$, the Hermitian Eqs. (3) do not allow for mode flux Φ to be trapped in a region surrounding the change in boundary conditions from a fluid-fluid to a no-slip interface. A minimal physical description of the fluid must account for the complete absorption of the mode K_2 through non-Hermitian physics.

Dissipative timescales— In addition to regularization, the effect of a nonzero viscosity ν in Eqs. (3) is to introduce length- and time-scales for both absorption and attenuation. Crucially, the absorption timescale for the trapped mode, $\tau_a \sim \omega^{-1}$, is set by the wave frequency independently from the dissipative viscosity. By contrast, the attenuation timescale τ_S for any transmitted mode was calculated by Stokes to be $\tau_S \sim c^2/(\omega^2 \nu)$ [90]. Because τ_S diverges when dissipation vanishes, for small viscosities absorption occurs much faster than attenuation, i.e., $\tau_a \ll \tau_S$. The region in which absorption occurs is defined by the legthscale $\ell \sim \sqrt{\nu/\omega}$, set by balancing the incoming energy flux $O(\omega|\mathbf{v}|^2)$ against dissipation $O(\nu |v|^2/\ell^2)$ due to velocity gradients v/ℓ . Even for vanishingly small but nonzero dissipative terms, the mode K_2 remains trapped inside this region, leading to complete absorption.

Outlook—We have demonstrated that when both timereversal symmetry and bulk-interface correspondence are broken, topological modes can flow into regions from which they cannot flow out. This reveals the non-Hermitian topology within any such system, because a minimal description for chiral edge states must include dissipative dynamics. These phenomena for chiral

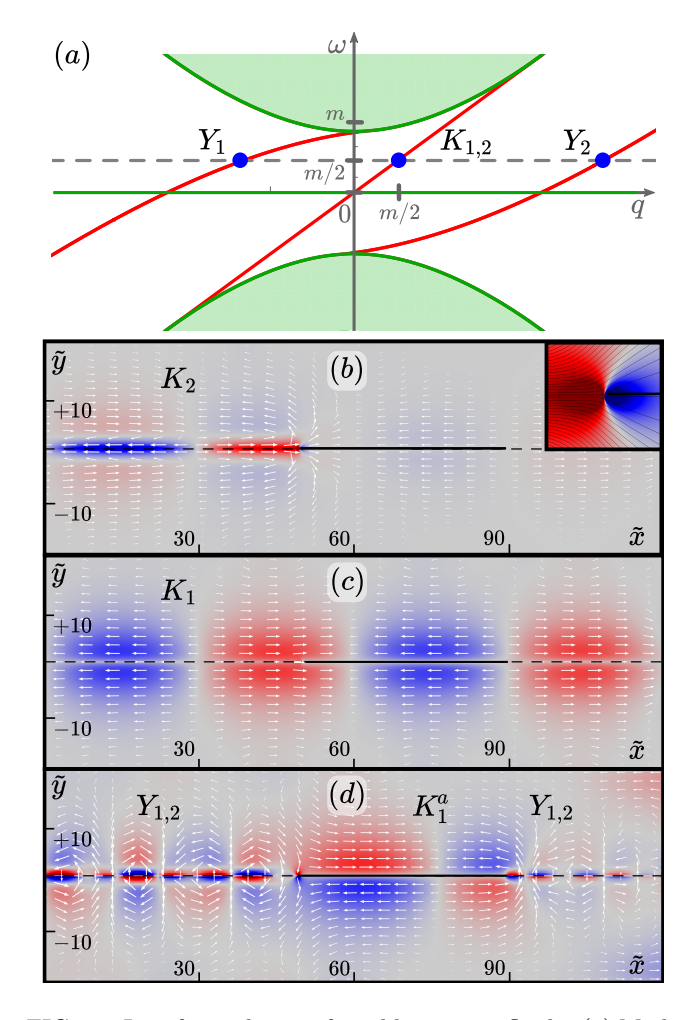


FIG. 3. Interface solutions for odd-viscosity fluids. (a) Mode spectrum for a chiral active fluid interface [Fig. 1(a)] showing the bulk (green) and interface (red) dispersion relations (m = 1/5). For a fluid-fluid interface, any frequency ω in the gap has four interface modes (blue points): two degenerate Kelvin modes (K_1, K_2) and two non-degenerate Yanai (Y_1,Y_2) modes. For the no-slip interface, only two degenerate Kelvin modes (K_1,K_1^a) exist, but no Yanai modes are present [c.f. Fig. 2(d)]. (b)-(d) Density (color) and velocity (arrows) of interface modes coming from the left along the fluid-fluid boundary (dashed line) and interacting with a finite-length segment of no-slip wall (solid black line). (b) The K_2 Kelvin wave is orthogonal to all waves supported on the no-slip wall and thus cannot be transmitted. The inset shows a zoom-in, including streamlines, near the change in boundary. (c) The K_1 Kelvin wave is supported on both interfaces and traverses the no-slip wall unaltered. (d) The antisymmetric Yanai waves map to the antisymmetric Kelvin mode K_1^a on the no-slip wall. Simulations were performed with parameters m = 0.2, D = 0, $\nu/\nu_0 = 0.01$.

edge modes can be constrasted with non-Hermitian skin modes and associated exceptional points [1–18]. Previously, chiral edge modes have been developed to construct robust waveguides for the conduction of electric current, light, or sound [19–21, 29–48]. Building on our

hydrodynamic model, topology could also be exploited to design perfect absorbers to completely shield against incoming signals.

Acknowledgments— P.A.M. gratefully acknowledges support through the Royal Society project IEC\R2\170195. A.S. gratefully acknowledges the support of the Engineering and Physical Sciences Research Council (EPSRC) through New Investigator Award No. EP/T000961/1.

- * a.souslov@bath.ac.uk
- [1] M. Brandenbourger, X. Locsin, E. Lerner, and C. Coulais, Nature communications 10, 1 (2019).
- [2] A. Ghatak, M. Brandenbourger, J. van Wezel, and C. Coulais, "Observation of non-hermitian topology and its bulk-edge correspondence," (2019), arXiv:1907.11619v1.
- [3] M. I. Rosa and M. Ruzzene, New Journal of Physics 22, 053004 (2020).
- [4] T. Helbig, T. Hofmann, S. Imhof, M. Abdelghany, T. Kiessling, L. Molenkamp, C. Lee, A. Szameit, M. Greiter, and R. Thomale, Nature Physics 16, 747 (2020).
- [5] T. Kotwal, H. Ronellenfitsch, F. Moseley, A. Stegmaier, R. Thomale, and J. Dunkel, arXiv preprint arXiv:1903.10130 (2019).
- [6] S. Weidemann, M. Kremer, T. Helbig, T. Hofmann, A. Stegmaier, M. Greiter, R. Thomale, and A. Szameit, Science 368, 311 (2020).
- [7] C. Scheibner, W. T. Irvine, and V. Vitelli, Physical Review Letters 125, 118001 (2020).
- [8] C. Scheibner, A. Souslov, D. Banerjee, P. Surowka, W. T. Irvine, and V. Vitelli, Nature Physics 16, 475 (2020).
- [9] D. Zhou and J. Zhang, Phys. Rev. Research 2, 023173 (2020).
- [10] H. Schomerus, Physical Review Research 2, 013058
- [11] J. C. Budich, J. Carlström, F. K. Kunst, and E. J. Bergholtz, Phys. Rev. B 99, 041406 (2019).
- [12] Y. Ashida, Z. Gong, and M. Ueda, "Non-hermitian physics," (2020), arXiv:2006.01837 [cond-mat.mes-hall].
- [13] Z. Gong, Y. Ashida, K. Kawabata, K. Takasan, S. Hi-gashikawa, and M. Ueda, Physical Review X 8, 031079 (2018).
- [14] T. Yoshida and Y. Hatsugai, Physical Review B 100, 054109 (2019).
- [15] S. Yao and Z. Wang, Physical review letters 121, 086803 (2018).
- [16] H. Shen, B. Zhen, and L. Fu, Phys. Rev. Lett. 120, 146402 (2018).
- [17] N. Hatano and D. R. Nelson, Phys. Rev. Lett. 77, 570 (1996).
- [18] C. M. Bender and S. Boettcher, Phys. Rev. Lett. 80, 5243 (1998).
- [19] M. Z. Hasan and C. L. Kane, Reviews of modern physics 82, 3045 (2010).
- [20] T. Kariyado and Y. Hatsugai, Scientific Reports 5, 1 (2015).
- [21] S. Shankar, M. J. Bowick, and M. C. Marchetti, Phys. Rev. X 7, 031039 (2017).

- [22] P. Delplace, J. Marston, and A. Venaille, Science 358, 1075 (2017).
- [23] J. E. Avron, R. Seiler, and P. G. Zograf, Phys. Rev. Lett. 75, 697 (1995).
- [24] J. E. Avron, Journal of Statistical Physics 92, 543 (1998).
- [25] S. R. D. Groot and P. Mazur, Non-Equilibrium Thermodynamics (Dover Publications, 1962) see in particular CH. XII, § 2.
- [26] D. Banerjee, A. Souslov, A. G. Abanov, and V. Vitelli, Nature communications 8, 1 (2017).
- [27] A. Berdyugin, S. Xu, F. Pellegrino, R. K. Kumar, A. Principi, I. Torre, M. B. Shalom, T. Taniguchi, K. Watanabe, I. Grigorieva, et al., Science 364, 162 (2019).
- [28] V. Soni, E. S. Bililign, S. Magkiriadou, S. Sacanna, D. Bartolo, M. J. Shelley, and W. T. Irvine, Nature Physics 15, 1188 (2019).
- [29] A. Souslov, K. Dasbiswas, M. Fruchart, S. Vaikuntanathan, and V. Vitelli, Physical review letters 122, 128001 (2019).
- [30] S. Shankar, A. Souslov, M. J. Bowick, M. C. Marchetti, and V. Vitelli, "Topological active matter," (2020), arXiv:2010.00364.
- [31] K. von Klitzing, Rev. Mod. Phys. 58, 519 (1986).
- [32] D. J. Thouless, M. Kohmoto, M. P. Nightingale, and M. den Nijs, Phys. Rev. Lett. 49, 405 (1982).
- [33] F. D. M. Haldane, Phys. Rev. Lett. 61, 2015 (1988).
- [34] M. C. Rechtsman, J. M. Zeuner, Y. Plotnik, Y. Lumer, D. Podolsky, F. Dreisow, S. Nolte, M. Segev, and A. Szameit, Nature 496, 196 (2013).
- [35] L. Lu, J. D. Joannopoulos, and M. Soljačić, Nature Photonics 8, 821 (2014).
- [36] V. Peano, C. Brendel, M. Schmidt, and F. Marquardt, Phys. Rev. X 5, 031011 (2015).
- [37] T. Ozawa, H. M. Price, A. Amo, N. Goldman, M. Hafezi, L. Lu, M. C. Rechtsman, D. Schuster, J. Simon, O. Zilberberg, et al., Reviews of Modern Physics 91, 015006 (2019).
- [38] L. M. Nash, D. Kleckner, A. Read, V. Vitelli, A. M. Turner, and W. T. M. Irvine, Proc. Natl. Acad. Sci. USA 112, 14495 (2015).
- [39] P. Wang, L. Lu, and K. Bertoldi, Phys. Rev. Lett. 115, 104302 (2015).
- [40] R. Süsstrunk and S. D. Huber, Science 349, 47 (2015).
- [41] A. B. Khanikaev, R. Fleury, S. H. Mousavi, and A. Alù, Nat Commun 6, 1 (2015).
- [42] Y.-T. Wang, P.-G. Luan, and S. Zhang, New Journal of Physics 17, 073031 (2015).
- [43] A. Souslov, B. C. van Zuiden, D. Bartolo, and V. Vitelli, Nature Physics 13, 1091 (2017).
- [44] K. Dasbiswas, K. K. Mandadapu, and S. Vaikuntanathan, Proceedings of the National Academy of Sciences 115, E9031 (2018).
- [45] N. P. Mitchell, L. M. Nash, D. Hexner, A. M. Turner, and W. T. M. Irvine, Nature Physics 14, 380 (2018).
- [46] R. Süsstrunk and S. D. Huber, PNAS 113, E4767 (2016).
- [47] S. D. Huber, Nature Physics 12, 621 (2016).
- [48] K. Bertoldi, V. Vitelli, J. Christensen, and M. Van Hecke, Nature Reviews Materials 2, 1 (2017).
- [49] T. Fukui, K. Shiozaki, T. Fujiwara, and S. Fujimoto, Journal of the Physical Society of Japan 81, 114602 (2012).
- [50] G. E. Volovik, Sov. Phys. JETP 67, 1804 (1988).
- [51] G. Bal, Journal of Mathematical Physics **60**, 081506

- (2019).
- [52] M. G. Silveirinha, Physical Review B **94**, 205105 (2016).
- [53] C. Tauber, P. Delplace, and A. Venaille, Phys. Rev. Research 2, 013147 (2020).
- [54] J. Dahler and L. Scriven, Nature **192**, 36 (1961).
- [55] J.-C. Tsai, F. Ye, J. Rodriguez, J. P. Gollub, and T. C. Lubensky, Phys. Rev. Lett. 94, 214301 (2005).
- [56] S. Fürthauer, M. Strempel, S. W. Grill, and F. Jülicher, Eur Phys J E 35, 89 (2012).
- [57] K. Drescher, K. C. Leptos, I. Tuval, T. Ishikawa, T. J. Pedley, and R. E. Goldstein, Physical Review Letters 102, 168101 (2009).
- [58] A. P. Petroff, X.-l. Wu, and A. Libchaber, Phys. Rev. Lett. 114, 158102 (2015).
- [59] J. Yan, S. C. Bae, and S. Granick, Soft Matter 11, 147 (2015).
- [60] J. Denk, L. Huber, E. Reithmann, and E. Frey, Phys. Rev. Lett. 116, 178301 (2016).
- [61] A. Snezhko, Current Opinion in Colloid and Interface Science 21, 65 (2016).
- [62] C. Maggi, F. Saglimbeni, M. Dipalo, F. D. Angelis, and R. D. Leonardo, Nat Commun 6, 8855 (2015).
- [63] M. Spellings, M. Engel, D. Klotsa, S. Sabrina, A. M. Drews, N. H. P. Nguyen, K. J. M. Bishop, and S. C. Glotzer, Proc. Natl. Acad. Sci. USA 112, E4642 (2015).
- [64] B. C. van Zuiden, J. Paulose, W. T. Irvine, D. Bartolo, and V. Vitelli, Proceedings of the national academy of sciences 113, 12919 (2016).
- [65] N. H. Nguyen, D. Klotsa, M. Engel, and S. C. Glotzer, Physical review letters 112, 075701 (2014).
- [66] K. Yeo, E. Lushi, and P. M. Vlahovska, Physical review letters 114, 188301 (2015).
- [67] G. Kokot, S. Das, R. G. Winkler, G. Gompper, I. S. Aranson, and A. Snezhko, Proceedings of the National Academy of Sciences 114, 12870 (2017).
- [68] C. del Junco, L. Tociu, and S. Vaikuntanathan, Proceedings of the National Academy of Sciences 115, 3569 (2018).
- [69] C. Scholz, M. Engel, and T. Pöschel, Nature communications 9, 1 (2018).
- [70] C. Tauber, P. Delplace, and A. Venaille, Journal of Fluid Mechanics 868, R2 (2019).
- [71] Technically, the modes mapped to zero are called the nullspace of \tilde{S} , and the dimensionality of the nullspace, called the nullity, must be at least Φ . Also note the distinction with mapping incoming waves into bound states, in which the scattering matrix remains unitary.
- [72] I. Rotter, Journal of Physics A: Mathematical and Theoretical 42, 153001 (2009).
- [73] S. Longhi, Physical review letters **105**, 013903 (2010).
- [74] A. Novitsky, D. Lyakhov, D. Michels, A. A. Pavlov, A. S. Shalin, and D. V. Novitsky, Physical Review A 101, 043834 (2020).
- [75] V. Achilleos, G. Theocharis, O. Richoux, and V. Pagneux, Physical Review B 95, 144303 (2017).
- [76] L. Feng, R. El-Ganainy, and L. Ge, Nature Photonics 11, 752 (2017).
- [77] J. Polchinski, in New Frontiers in Fields and Strings: TASI 2015 Proceedings of the 2015 Theoretical Advanced Study Institute in Elementary Particle Physics (World Scientific, 2017) pp. 353–397.
- [78] M. Kaminski and S. Moroz, Physical Review B 89, 115418 (2014).

- [79] T. Markovich and T. C. Lubensky, "Odd viscosity in active matter: microscopic origin and 3d effects," (2020), arXiv:2006.05662 [cond-mat.soft].
- [80] G. E. Volovik, Soviet Physics Uspekhi 27, 363 (1984).
- [81] I. V. Tokatly and G. Vignale, Physical Review B 76, 161305 (2007).
- [82] N. Read and E. H. Rezayi, Physical Review B 84, 085316 (2011).
- [83] B. Offertaler and B. Bradlyn, Physical Review B 99, 035427 (2019).
- [84] J. Korving, H. Hulsman, H. Knaap, and J. Beenakker, Physics Letters 21, 5 (1966).
- [85] H. Knaap and J. Beenakker, Physica **33**, 643 (1967).
- [86] S. L. Rosenthal, Monthly Weather Review 93, 605 (1965).
- [87] T. Matsuno, Journal of the Meteorological Society of Japan. Ser. II 44, 25 (1966).
- [88] M. Yanai and T. Maruyama, Journal of the Meteorological Society of Japan. Ser. II 44, 291 (1966).
- [89] P. A. Milewski and E. G. Tabak, Geophysical & Astrophysical Fluid Dynamics 90, 139 (1999).
- [90] L. Landau and E. Lifshitz, "Fluid mechanics: Volume 6," (Elsevier Science, 2013) Chap. 8, pp. 300–303.
- [91] P. Wiegmann and A. G. Abanov, Phys. Rev. Lett. 113, 034501 (2014).
- [92] M. Han, M. Fruchart, C. Scheibner, S. Vaikuntanathan, W. Irvine, J. de Pablo, and V. Vitelli, "Statistical mechanics of a chiral active fluid," (2020), arXiv:2002.07679.
- [93] A. Souslov, A. Gromov, and V. Vitelli, Physical Review E 101, 052606 (2020).

Complete absorption of topologically protected waves: Supplemental Material

Odd viscosity in fluids of spinning particles

In this section, we review the hydrodynamic origins of Eqs. (3) as a description of acoustic waves in twodimensional chiral active fluids [26, 29, 79]. Consider an ideal fluid of spinning particles, subject to a Coriolis (equivalently, Lorentz) body force. The equation of motion in terms of the mass density $\rho(x, y, t)$ and fluid flow $\boldsymbol{v}(x, y, t)$ is

$$\partial_t(\rho \mathbf{v}) + \nabla \cdot [\rho \mathbf{v} \otimes \mathbf{v} - \underline{\boldsymbol{\sigma}}] = \Omega_B \rho \mathbf{v}^*,$$
 (6)

where the * operator acts on vectors $\mathbf{v} = (u, v)$ as $(u, v)^* = (-v, u)$, and the stress tensor is given by

$$\sigma_{ij} = -p\delta_{ij} + \eta^{o}(\partial_{i}v_{j}^{*} + \partial_{i}^{*}v_{j}) + \eta(\partial_{i}v_{j} + \partial_{j}v_{i} - \partial_{k}v_{k}\delta_{ij}),$$
(7)

where p is the pressure, η is the (dynamic) dissipative shear viscosity, and η^o is the (dynamic) odd viscosity, with kinematic viscosities used in the text defined by $\nu^o = \eta^o/\rho_0$ and $\nu = \eta/\rho_0$. Although we do not include the dissipative bulk viscosity term $\zeta \partial_k v_k \delta_{ij}$ in the stress tensor, qualitatively this term would not affect our conclusions. Both the dissipative and odd viscosities arise from the same viscosity tensor η_{ijkl} , defined as rank-4 tensor that linearly relates the rank-2 stress tensor to the rank-2 strain rate tensor, $\sigma_{ij} = \eta_{ijkl} \partial_k v_l$. The difference is that the part of the viscosity tensor η^e_{ijkl} containing dissipative viscosity is even under time-reversal symmetry and therefore (by Onsager reciprocity relations) has to satisfy $\eta_{ijkl}^e = \eta_{klij}^e$, i.e., the dissipative viscosity enters the even part of the viscosity tensor under the exchange $ij \leftrightarrow kl$. By contrast, the part of the viscosity tensor η_{ijkl}^o that contains odd viscosity is odd under time-reversal symmetry and therefore has to satisfy $\eta_{ijkl}^o = -\eta_{klij}^o$, i.e., the odd viscosity enters the odd part of the viscosity tensor under the exchange $ij \leftrightarrow kl$. A peculiar property that arises from the symmetry of odd viscosity is that this term does not lead to energy dissipation, as can be checked directly by evaluating the entropy production rate as $\frac{1}{2}\eta_{ijkl}^{o}\partial_{i}v_{j}\partial_{k}v_{l}=0$. Because odd viscosity must break time-reversal symmetry, this term naturally arises in systems with an external magnetic field or rotation. In chiral active fluids, the intrinsic rotation of each individual particle gives rise to this term.

General arguments for the value of odd viscosity can be made in cases in which the spinning particles composing the fluid are weakly interacting, $\eta^o = \pm \ell/2$, where ℓ is the density of the intrinsic angular momentum for the individual particles. The \pm sign in the relation depends on the microscopic origins of the effect [26, 79, 91]. For some chiral active fluids with inertia, $\ell = I\Omega_A$, where each particle rotates with intrinsic angular velocity Ω_A with I the individual particles' moment of inertia times

the fluid density [26, 29]. In a variety of fluids, odd viscosity arises due to interparticle interactions [92] and dissipative processes [93], rendering it a distinct transport coefficient independent of the intrinsic angular momentum ℓ . For simplicity, we choose to define the chiral terms via the frequencies Ω_A and Ω_B , which act as proxies for the magnitude of the chiral body force and odd viscosity, respectively. We will consider only cases where in the bulk of the fluid these two quantities have the same non-zero sign, i.e., $\Omega_A = s|\Omega_A|$ and $\Omega_B = s|\Omega_B|$ with $s = \pm 1$.

We linearize Eq. (6) together with the continuity equation $\partial_t \rho + \nabla \cdot (\rho v) = 0$ around $\rho = \rho_0$ and v = 0 to obtain Eq. (3) in the main text. We use $\eta^o = I\Omega_A/2$, $c^2 = \partial p/\partial \rho$, and choose units of mass density in terms of ρ_0 , length in terms of $I\Omega_A/(2c\rho_0)$, and time in terms of $I\Omega_A/(2c^2\rho_0)$. In these units, (kinematic) dissipative viscosity ν is measured in units of the (kinematic) odd viscosity ν^o . This non-dimensionalized system is controlled by the discrete constant $s = \pm 1$ and the positive constant $m = |I\Omega_A\Omega_B|/(2\rho_0c^2)$, which is assumed to satisfy m < 1/4 to ease later computation.

We note that the linearized equations conserve the (rescaled) energy $E = \rho^2 + ||\boldsymbol{v}||^2$, which can be seen by deriving the energy continuity equation

$$\partial_t \int_V E \, dA = -2 \int_{\partial V} \hat{\boldsymbol{n}} \cdot \underline{\boldsymbol{\sigma}} \cdot \boldsymbol{v} \, d\ell. \tag{8}$$

Suppose that we have two regions V_1 and V_2 which share a piece of their boundary ∂V_{12} (= $\partial V_1 \cap \partial V_2$). For the energy E to be conserved, we need the flux out of V_1 to equal the flux into V_2 and vice-versa. That is, the flux $\hat{\boldsymbol{n}} \cdot \underline{\boldsymbol{\sigma}} \cdot \boldsymbol{v}$ needs to be continuous at ∂V_{12} . There are two natural ways to guarantee that to $\hat{\boldsymbol{n}} \cdot \underline{\boldsymbol{\sigma}} \cdot \boldsymbol{v}$ is continuous, namely (1) Stress-continuity: continuous \boldsymbol{v} and continuous $\hat{\boldsymbol{n}} \cdot \underline{\boldsymbol{\sigma}}$; or (2) Velocity-vanishing: continuous \boldsymbol{v} and $\boldsymbol{v}|_{\partial V_{12}} = 0$. Case (1) governs the dynamics of the fluid bulk and fluid-fluid interfaces. Case (2) governs the dynamics where the fluid touches a no-slip wall.

Bulk solutions

In this section, we review the evaluation of Chern number within the dispersion relation associated with Eqs. (3) [29, 51, 70]. We can write Eqs. (3) as a Hamiltonian equation $-i\partial_t \psi = H_s(i\partial_x, i\partial_y)\psi$ in terms of $\psi = (\rho, u, v)^T$, where

$$H_s(i\nabla) = \begin{pmatrix} 0 & i\partial_x & i\partial_y \\ i\partial_x & 0 & -is\left(m - (i\nabla)^2\right) \\ i\partial_y & +is\left(m - (i\nabla)^2\right) & 0 \end{pmatrix}$$
(9)

In the bulk, the Hamiltonian commutes with all time and space derivatives, so we may assume bulk waves of the form $\psi = \Psi e^{i(\omega t - q \cdot x)}$. The Hamiltonian equation then reduces to a family of eigenvalue equations $H_s(q)\Psi = \omega \Psi$, with:

$$\omega_0(\mathbf{q}) = 0 \quad \text{or} \quad \omega_{\pm}(\mathbf{q}) = \pm \sqrt{\lambda^2 + q_x^2 + q_y^2},$$
 (10)

where $\lambda(\mathbf{q}) = m - q_x^2 - q_y^2$, and eigenvectors

$$\Psi_0(\mathbf{q}) \propto \begin{pmatrix} \lambda \\ iq_y \\ -iq_x \end{pmatrix}, \quad \Psi_{\pm}(\mathbf{q}) \propto \begin{pmatrix} iq_y\lambda + q_x\omega_{\pm} \\ q_x^2 + \lambda^2 \\ q_xq_y + i\lambda\omega_{\pm} \end{pmatrix}. \quad (11)$$

Significantly, this orthogonal basis is well-defined over the compactified plane of wavevectors q, for which all of the points at infinity are identified.

The Chern number for the lower band, which determines the number and chirality of modes in systems satisfying bulk-boundary correspondence, can be evaluated from the Berry curvature. The Berry curvature of each band in Eq. (11) is a function of the wavevector \boldsymbol{q} given by

$$\mathcal{B}(\mathbf{q}) = i \nabla_{\mathbf{q}} \times [\mathbf{\Psi}^{\dagger}(\mathbf{q}) \cdot \nabla_{\mathbf{q}} \mathbf{\Psi}(\mathbf{q})], \tag{12}$$

where the dot product contracts eigenvector components, whereas the gradient and curl are vectors in \mathbf{q} -space. Here $\mathcal{B}_0 = 0$ is trivial, leaving $\mathcal{B}_+ = -\mathcal{B}_-$. Integrating the Berry curvature over all of wavevector space gives the Chern number for the lowest band [29, 51],

$$C_{-} = \frac{1}{2\pi} \int \mathcal{B}_{-} d\mathbf{q} = \operatorname{sgn}(\Omega_{A}) + \operatorname{sgn}(\Omega_{B}) = 2s, \quad (13)$$

which determines the number of edge states when the bulk-boundary correspondence holds.

Half spaces

Now suppose our space is partitioned by a boundary along y=0 into an upper (y>0) and lower (y<0) halfspace where, respectively, $s_{\uparrow}=+1$ and $s_{\downarrow}=-1$. Because of the discontinuity in s, Eq. (3) is ill-defined at the interface y=0. We proceed by solving the PDE on the upper (lower) halfspace separately to obtain general solutions $\psi_{\uparrow}(\psi_{\downarrow})$. We will stitch these solutions together with interface conditions along y=0.

Since the PDE is linear with constant coefficients on each halfspace, we may decompose the solutions in exponentials:

$$\psi_{\uparrow} = \Psi_{\uparrow} e^{-\kappa_{\uparrow}|y|} e^{i(\omega t - qx)}. \tag{14}$$

To ensure localization, we require $\operatorname{Re} \kappa_{\uparrow} > 0$. We proceed by fixing a pair $(\omega, q) \in \mathbb{R}^2$, with ω in the gap, and checking for complex solutions Ψ_{\uparrow} and κ_{\uparrow} at each pair (ω, q) .

The Hamiltonian equation now reads $H(q, -is_{\uparrow}\kappa_{\uparrow})\Psi_{\uparrow} = \omega\Psi_{\uparrow}$, with

$$H(q, -is\kappa) = \begin{pmatrix} 0 & q & -is\kappa \\ q & 0 & -is\lambda \\ -is\kappa & +is\lambda & 0 \end{pmatrix}, \tag{15}$$

and $\lambda = m - q^2 + \kappa^2$. The characteristic equation $\det[H(q, -is_{\uparrow}\kappa_{\uparrow}) - \omega] = 0$ is independent of s_{\uparrow} , thus κ_{\uparrow} has the same values on the top and bottom halfspaces and we may drop the arrow subscript. Assuming $\omega \neq 0$, the characteristic equation has four solutions for κ :

$$4\left(\kappa_{\pm}\right)^{2} = 1 \pm 2\Gamma(\omega) + \Gamma^{2}(q),\tag{16}$$

where we use the shorthand $\Gamma(x) \equiv \sqrt{1-4m+4x^2}$, which is real and positive by our assumption m < 1/4. Since solutions to Eq. (16) come in \pm pairs, we always find exactly two solutions with Re $\kappa_{\pm} < 0$ that diverge as $y \to \infty$, and two with Re $\kappa_{\pm} > 0$ that are localized. In particular, one can show that the right-hand side of Eq. (16) is positive for every ω in the gap. Thus, the admissible κ are

$$\kappa_{\pm}(\omega, q) = \frac{1}{2}\sqrt{1 \pm 2\Gamma(\omega) + \Gamma^2(q)}.$$
 (17)

For these κ_{\pm} , the parameter λ from Eq. (15) takes values $\lambda_{\pm}(q,\omega) = \kappa_{\pm}(\omega,\omega)$. The corresponding eigenvectors on the two half-spaces can then be denoted as

$$\Psi_{\updownarrow}^{\pm}(\omega,q) \propto \begin{pmatrix} \kappa_{\pm}\lambda_{\pm} + q\omega \\ \kappa_{\pm}^{2} + \omega^{2} \\ is_{\uparrow}(\omega\lambda_{\pm} - q\kappa_{\pm}) \end{pmatrix} = \begin{pmatrix} R^{\pm} \\ U^{\pm} \\ is_{\uparrow}V^{\pm} \end{pmatrix}. \quad (18)$$

These can be quickly checked against Eq. (15) using $\kappa_{\pm}^2 - \lambda_{\pm}^2 = q^2 - \omega^2$. The general solutions on the two half-spaces can then be written as

$$\psi_{\uparrow} = \sum_{+} A_{\uparrow}^{\pm} \Psi_{\uparrow}^{\pm} e^{-\kappa_{\pm}|y|} e^{i(\omega t - qx)}, \tag{19}$$

with four complex coefficients A_{\uparrow}^+ , A_{\uparrow}^- , A_{\downarrow}^+ and A_{\downarrow}^- , which have to be fixed by the interface condition.

No-slip interface modes

The velocity-vanishing condition on the no-slip wall reads $[u] = [v] = \bar{u} = \bar{v} = 0$. Recall that $\psi = (\rho, u, v)$, and that the jump and average of a function f(y) at y = 0 are defined as $[f] = f_{\uparrow}(0) + f_{\downarrow}(0)$ and $2\bar{f} = f_{\uparrow}(0) + f_{\downarrow}(0)$ respectively. Substituting Eq. (19), we can write this condition as a matrix equation

$$\begin{pmatrix} \mathbf{0} \\ \mathbf{0} \end{pmatrix} = \begin{pmatrix} M & -M \\ M & M \end{pmatrix} \begin{pmatrix} \mathbf{A}_{\uparrow} \\ \mathbf{A}_{\downarrow} \end{pmatrix} = \begin{pmatrix} M(\mathbf{A}_{\uparrow} - \mathbf{A}_{\downarrow}) \\ M(\mathbf{A}_{\uparrow} + \mathbf{A}_{\downarrow}) \end{pmatrix}, \quad (20)$$

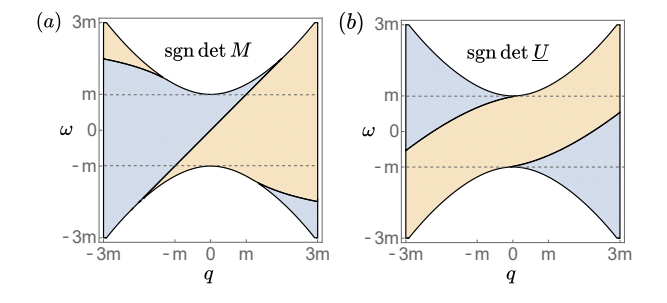


FIG. 4. Invertibility of submatrices that determine the interface conditions. The determinants are real between the bulk curves $\omega = \omega_{\pm}(q)$. Interface waves exist along the curves where the determinant changes from negative (blue) to positive (yellow). (a) For the no-slip interface, $\det M = 0$ has only one doubly degenerate Kelvin solution for every ω in the gap (dashed lines). (b) For the fluid-fluid interface, $\det \underline{U} = 0$ gives two singly degenerate Yanai curves, in addition to the doubly degenerate Kelvin curve $\omega = q$ (not depicted) corresponding to $\det \underline{V} = 0$.

on the block vectors $\mathbf{A}_{\updownarrow} = (A_{\updownarrow}^+, A_{\updownarrow}^-)^T$, where the submatrix M depends on (ω, q) through $\mathbf{\Psi}_{\updownarrow}^{\pm}$ as

$$M = \begin{pmatrix} U^+ & U^- \\ iV^+ & iV^- \end{pmatrix}. \tag{21}$$

Thus the interface condition is satisfied if and only if $M\mathbf{A}_{\uparrow} = M\mathbf{A}_{\downarrow} = \mathbf{0}$. In particular, we only find non-zero solutions at those (ω, q) for which $\det M(\omega, q) = 0$.

First let us assume $\omega=q$. Then $\lambda_{\pm}=\kappa_{\pm}$ and, by Eq. (18), $R^{\pm}=U^{\pm}\neq 0$ and $V^{\pm}=0$. In other words, the velocity normal to the boundary vanishes (v=0), and the density equals the tangent velocity $(\rho=u)$. Since only the second row of M vanishes, the two zero-eigenvectors \mathbf{A}_{\uparrow} have to be colinear, but we can choose their sign and magnitude independently. In particular we may take an orthogonal basis with one even $(\mathbf{A}_{\uparrow}=\mathbf{A}_{\downarrow})$ and one odd solution $(\mathbf{A}_{\uparrow}=-\mathbf{A}_{\downarrow})$ about y=0. We can write these solutions as $\psi=(1,1,0)^TK(y)e^{i\omega(t-x)}$ where the two y-profiles are

$$K_1 = \sinh\left(\frac{1}{2}\Gamma|y|\right)$$
 and $K_1^a = \sinh\left(\frac{1}{2}\Gamma y\right)$. (22)

These waves with flow parallel to the interface are known as *Kelvin waves*. No zero-eigenvectors for $M(\omega, q)$ exist at other (ω, q) in the gap, as shown in Fig. 4(a).

Fluid-fluid interface modes

The stress-continuity condition on the fluid-fluid interface reads in vectorial form $[v] = 0 = [\hat{y} \cdot \underline{\sigma}]$. The latter of which can be expanded with

$$(\hat{\boldsymbol{y}} \cdot \underline{\boldsymbol{\sigma}})_j = \delta_{2i} (-\rho \delta_{ij} - s \partial_i v_j^{\perp}) = (s \partial_y v, -s \partial_y u - \rho)_j.$$
(23)

Again, substituting Eq. (19) gives us a block matrix equation

$$\begin{pmatrix} \mathbf{0} \\ \mathbf{0} \end{pmatrix} = \begin{pmatrix} \underline{U} & -\underline{U} \\ i\underline{V} & i\underline{V} \end{pmatrix} \begin{pmatrix} \mathbf{A}_{\uparrow} \\ \mathbf{A}_{\downarrow} \end{pmatrix} = \begin{pmatrix} \underline{U}(\mathbf{A}_{\uparrow} - \mathbf{A}_{\downarrow}) \\ i\underline{V}(\mathbf{A}_{\uparrow} + \mathbf{A}_{\downarrow}) \end{pmatrix}, \quad (24)$$

with submatrices

$$\underline{U} = \begin{pmatrix} U^+ & U^- \\ \kappa_+ U^+ - R^+ & \kappa_- U^- - R^- \end{pmatrix}$$
 (25)

and

$$\underline{V} = \begin{pmatrix} V^+ & V^- \\ \kappa_+ V^+ & \kappa_- V^- \end{pmatrix}. \tag{26}$$

This last matrix \underline{V} is singular if and only if $\omega=q$. To see this, note that κ_- never equals κ_+ , since $\Gamma(\omega)>0$. Thus $\det \underline{V}=0$ requires either V^+ or V^- to vanish, which happens if and only if $\omega\lambda_\pm=q\kappa_\pm$. Since λ_\pm and κ_\pm are both positive, we know that $\omega q\geq 0$ and we may proceed to square both sides to obtain:

$$0 = \omega^{2} (1 \pm \Gamma(\omega))^{2} - q^{2} (1 \pm 2\Gamma(\omega) + \Gamma^{2}(q))$$

= $(\omega^{2} - q^{2}) [(1 \pm \Gamma(\omega))^{2} + 4q^{2}].$ (27)

The expression in square brackets is strictly nonzero, as $\Gamma(\omega)=1$ requires $|\omega|=\sqrt{m}>m$, which is outside the gap. In conclusion, either $\omega=q$ and $V^+=V^-=0$, or $\omega\neq q$ and V^+,V^- are both non-zero. On the other hand, $\det \underline{U}$ vanishes along two curves that do not cross $\omega=q$, but are in the gap, as shown in Fig. 4(b).

First, we again look at Kelvin waves along $\omega = q$. Here, \underline{V} is the zero-matrix and \underline{U} is invertible, thus by Eq. (24), our solutions are even $(A_{\downarrow} = A_{\uparrow})$, but further unconstrained. This two-dimensional space of Kelvin waves can be spanned by functions $\psi = (1,1,0)^T K(y) e^{i\omega(t-x)}$ with hyperbolic functions as y-profiles:

$$K_s = \sinh\left(\frac{1}{2}\Gamma|y|\right)$$
 and $K_c = \cosh\left(\frac{1}{2}\Gamma|y|\right)$. (28)

We can orthogonalize this set as:

$$K_1 = K_s$$
 and $K_2 = K_s - K_c/\Gamma$. (29)

The first is identical to the K_1 mode on the no-slip interface, while the second is orthogonal to both modes on the no-slip interface.

In contrast to the no-slip interface, the fluid-fluid interface has boundary waves in the gap which do not lie along the line $\omega=q$. Since for these modes \underline{V} is invertible, we see from Eq. (24) that solutions must satisfy $\mathbf{A}_{\downarrow}=-\mathbf{A}_{\uparrow}$. Consequently, ρ and u are odd about y=0. Furthermore, v is related to \mathbf{A} with prefactor is_{\uparrow} (see Eq. (18)), thus v will be even and 90° out of phase with both u and ρ . This suggests a rotational flow for these so-called $Yanai\ waves$, in contrast with the parallel flow of Kelvin waves.

These Yanai modes must satisfy $\underline{U} A_{\uparrow} = \mathbf{0}$. Looking at the top row of \underline{U} , and knowing that $U^{\pm} \neq 0$ from Eq. (18), we see that $A_{\uparrow} = -A_{\downarrow} = (-U^-, +U^+)$. Thus along each line we find one non-degenerate mode Y_1^o and Y_2^o , which we can write as

$$\psi_{\uparrow} = s_{\uparrow} \left(U_{+} \Psi_{\uparrow}^{+} e^{-\kappa_{+}|y|} - U_{-} \Psi_{\uparrow}^{-} e^{-\kappa_{-}|y|} \right) e^{i(\omega t - qx)}. \tag{30}$$

The two modes are differentiated by the two Yanai dispersion curves $\omega(q)$, for which we do not find a closed-form solution. Approximate values for this dispersion relation may be computationally obtained and plugged into Eqs. (16,18) to obtain numerical solutions.